Glide back recovery of a winged reusable launch vehicle with wind estimate

Prince Edorh, Bruno Hérissé, Eric Bourgeois

Glide back recovery of a winged reusable launch vehicle with wind estimate

Prince Edorh⋆*, Bruno Hérissé*⋆ *and Eric Bourgeois*†
⋆*DTIS, ONERA, Université Paris Saclay, F-91123 Palaiseau, France*
prince.edorh@gmail.com · bruno.herisse@onera.fr
† *CNES - 52, rue Jacques Hillairet, 75012 Paris, France*
eric.bourgeois@cnes.fr

Abstract

The development of future launchers leads CNES and ONERA to be interested in concepts of winged vehicles with horizontal landing. From the experience acquired on the vertical takeoff vertical landing (VTVL) concept, a glide back recovery concept is studied in this paper using a similar control approach. It involves a guidance algorithm which relies on an indirect optimal control method based on the Pontryagin maximum principle. Glide back recoveries expose the winged vehicle to wind disturbances. Therefore, the guidance model incorporates wind management. The wind profile is estimated onboard the vehicle using an extended Kalman filter. Promising results have shown that this approach can be deployed in realistic flight conditions.

1. Introduction

Commercial and scientific interests in partially or fully reusable launchers have increased considerably in recent years. Among various strategies which enable the recovery of the first stage of Reusable Launch Vehicles, the glide back return (Figure 1) emerges as a promising alternative to the toss-back concept.[4,9] While the latter has proved its worth on SpaceX Falcon 9 launchers, the former offers a more cost-effective solution in terms of both propellant consumption and ground infrastructure costs.[3] For a toss back recovery, a large amount of energy is lost to make the vehicle turn over. Instead, the glide back, which is designed for winged vehicles, exploits the aerodynamic capacities of the vehicle to minimize the amount of energy to be consumed. Such strategy enables a horizontal landing which can be thus performed on an existing runway, close to the launch site. Moreover, the recovery of a winged first stage must be carried out while ensuring constraints on the dynamic pressure, the heat flow, the load factors, and the atmospheric re-entry. A robust and efficient guidance algorithm is then required as the vehicle's aerodynamic performance is extremely sensitive to its environment (e.g., wind, air density, atmospheric pressure). Wind disturbances play an important role in vehicle dynamics and they should be taken into consideration. This paper thus provides a numerical guidance algorithm which computes online and in real time the optimal recovery trajectory of a winged vehicle from the stage separation to the landing maneuver, while minimizing propellant mass consumption.

The recovery of the vehicle is described as an optimal control problem which is solved with an indirect shooting method based on the Pontryagin's maximum principle. By augmenting the state of the system and its dynamics with a costate, we derive a set of necessary conditions of optimality, written as a zero-finding problem, that can be quickly solved by a Newton-like algorithm. The optimal control problem then consists in finding the correct initialization of the costate. First, a reference trajectory is computed offline to provide a first solution to the problem. This trajectory consists of a unique thrust maneuver (that cancels out the horizontal component of the vehicle's velocity) and an unpowered atmospheric re-entry which encompasses several turn maneuvers. Then, with this solution as an initial guess, the guidance algorithm recomputes online the optimal control using the true current state of the vehicle at each time.

With such an approach, highly accurate solutions are quickly provided, at a frequency that is compatible with actual embedded guidance components. Additionally, the guidance law has been found sufficiently robust to accommodate various uncertainties on parameters (e.g. initial state at the beginning of the recovery procedure, rocket engine, aerodynamic coefficients). The introduction of wind in the atmospheric and aerodynamic models will particularly impact the handling of the first stage during its descent. While the guidance model, that does not take into account any knowledge of the wind profile, is quite effective in the absence of strong wind gusts, we propose to include wind information in the guidance design to obtain a more robust solution. To this purpose, a wind estimation

based on an extended Kalman filter (EKF) is added in the navigation component of the GNC loop. Then, this estimate is injected in the model based guidance algorithm.

The paper is organized as follows. In Section 2, the guidance algorithm based on an indirect shooting method is introduced. Section 3 briefly presents the strategy for wind estimation. Section 4 provides some numerical results to demonstrate the effectiveness of the full navigation and guidance algorithm.

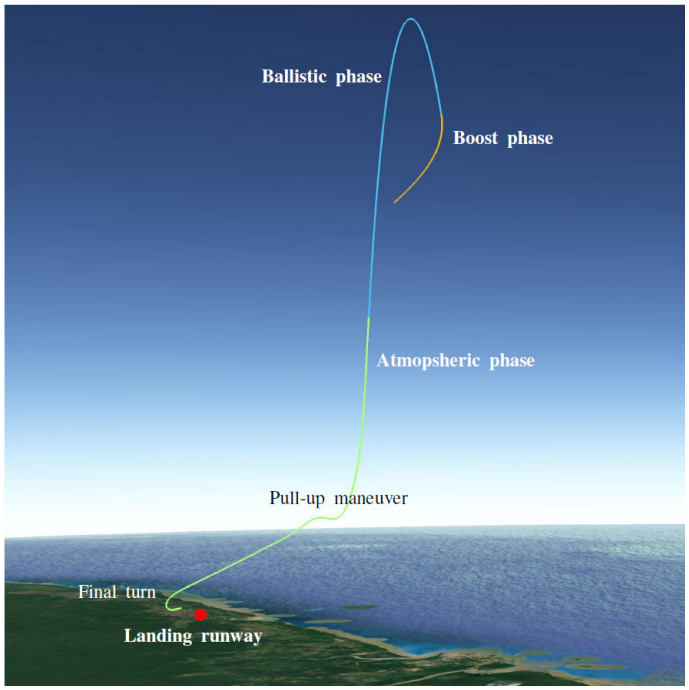

Figure 1: Illustration of a glide-back recovery trajectory of a reusable launch vehicle.

2. Guidance component

A promising closed-loop guidance algorithm dedicated to the recovery of a vertical take-off and vertical landing (VTVL) vehicle has been introduced in a previous work.[9] Their approach consists of solving periodically an optimal control problem that describes the vehicle motion throughout the recovery. The initial conditions of the problem are given by the current state of the vehicle and thus evolve periodically. The guidance loop is initialized with a reference solution computed offline. This trajectory is then updated throughout the flight with the current flight data (Figure 2).

As the solution is computed with an underlying iterative method, the latest computed solution is used as an initial guess for the current optimal control problem. The advantage of such an approach is to defer most of the computation to the pre-flight phase. The reference trajectory is computed by solving an optimal control problem whose initial conditions correspond to an estimate of the first stage configuration at stage separation. The vehicle dynamics are reproduced by a dynamical model that is accurate enough to overcome any in-flight uncertainty while remaining relatively simple in order to provide at anytime a computable control.

For the present work, we adapt the guidance scheme in order to recover a vertical take-off and horizontal landing (VTHL) vehicle in presence of wind. Our dynamical model extends the previous model[9] by including the effect of a constant wind profile all along the flight (see Section 2.1). Based on this model, we derive an optimal control problem that can be suitable for the recovery of a winged vehicle (see Section 2.2). Due to the possible cornering maneuvers at reentry, such an optimal control problem must incorporate constraints on the lateral load factor of the vehicle. Fortunately, this optimal control problem can be solved with an indirect approach through an application of Pontryagin's Maximum Principle (PMP). The derivation of an optimal solution can be found in Section 2.3 where we exploit the structure of the solution. It allows us to derive an off-line trajectory with zero wind. The onboard guidance is then initialized with this reference solution. For each in-flight re-computation, the guidance algorithm assumes for the remaining of the flight a constant wind profile (magnitude and direction) provided by the navigation component. The current flight data then embeds the current state of the vehicle as well as a wind estimation provided by the navigation component (Figure 2). A new solution is then computed by solving an updated optimal control problem. Numerically, two continuation procedures[14] are utilized in order to evaluate the new solution based on the latest computation. The

first is carried out on the vehicle initial state, followed by a continuation on the wind profile. The resulting control input is then used until the following recalculation.

In the upcoming subsections, we briefly describe the key elements used by the guidance component. Then, Section 3 will describe the navigation component which performs the estimation of the instantaneous wind acting on the vehicle.

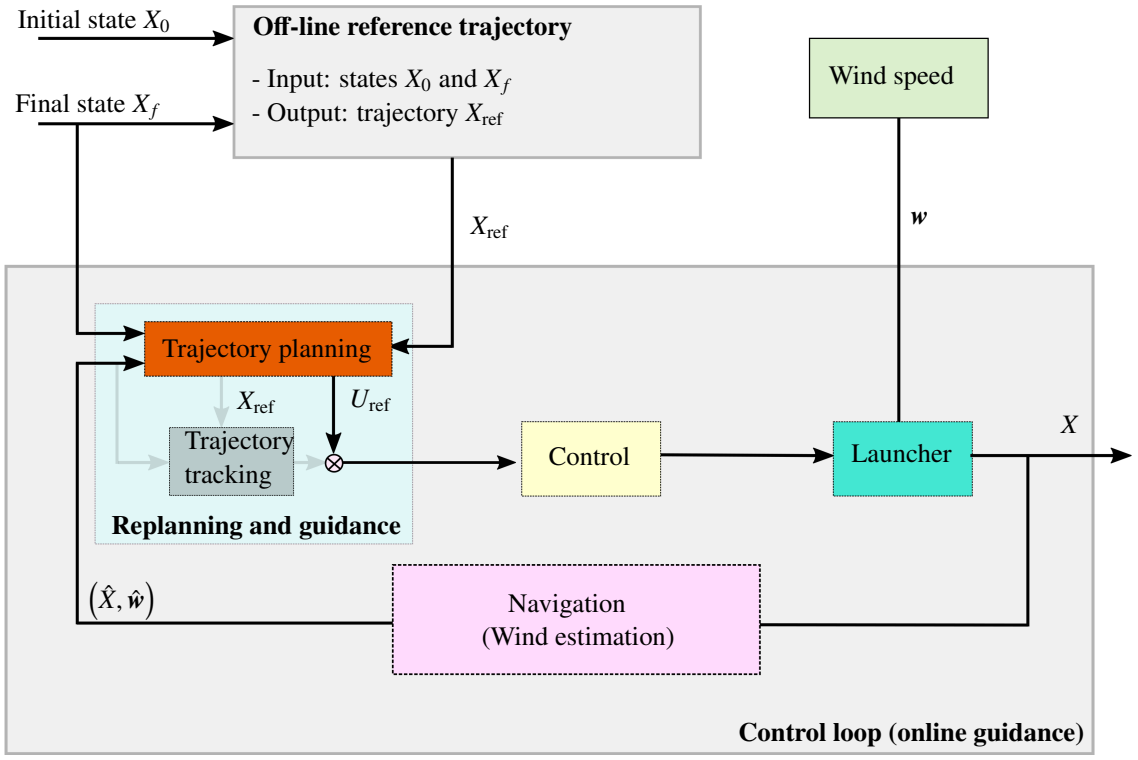

Figure 2: Guidance, Navigation and Control scheme bypassing trajectory tracking (replanning only).

2.1 Dynamical model

Let us consider a reusable VTHL vehicle whose state is denoted by its mass m, its position $\boldsymbol{r}$ and its velocity $\boldsymbol{v}$. We assume, for now, that a constant wind profile $\boldsymbol{w}$ is applied to the vehicle throughout the atmospheric phase. The motion of such vehicle can be described in the Earth-centered, Earth-fixed frame by the following dynamics

$$\begin{pmatrix} \dot{\boldsymbol{r}} \\ \dot{\boldsymbol{v}} \\ \dot{m} \end{pmatrix} = \begin{pmatrix} \boldsymbol{v} \\ \boldsymbol{a} - 2\boldsymbol{\Omega} \times \boldsymbol{v} - \boldsymbol{\Omega} \times (\boldsymbol{\Omega} \times \boldsymbol{r}) \\ -q_m \Lambda \end{pmatrix}, \tag{1}$$

where $\boldsymbol{\Omega}$ denotes the Earth's rotational velocity, Λ is normalized engine throttle control and q_m is the maximal mass flow rate. Here, the acceleration due to thrust, aerodynamic and gravity forces is given by

$$\boldsymbol{a} = \Lambda \frac{T(r)}{m} \mathbf{1}_{\boldsymbol{b}} - \frac{D(\boldsymbol{r}, \boldsymbol{v} - \boldsymbol{w}, \alpha)}{m} \mathbf{1}_{\boldsymbol{v}-\boldsymbol{w}} + \frac{L(\boldsymbol{r}, \boldsymbol{v} - \boldsymbol{w}, \alpha)}{m} \mathbf{1}_{\boldsymbol{k}} - \boldsymbol{g}(\boldsymbol{r}). \tag{2}$$

The gravity vector reads $\boldsymbol{g}(r) = \mu_0 \boldsymbol{r} / \|\boldsymbol{r}\|^3$ where μ_0 denotes the Earth's gravitational constant.
The thrust force is given as a function of the maximal thrust (which depends on the maximal mass flow rate of the engine and the specific impulse), the nozzle exit area of the switched on engines and the ambient pressure

$$T(r) = T_{\max} - S_{\text{exit}} P_a(\boldsymbol{r}). \tag{3}$$

We here assume the orientation dynamics fast enough to be neglected in the modeling of the guidance design. Then, the orientation of the thrust is $\mathbf{1}_{\boldsymbol{b}}(t) \in \mathbb{R}^3$, a unit vector which defines the launcher body longitudinal axis, while $\Lambda(t) \geqslant 0$ corresponds to the normalized thrust ($|\Lambda| \leq 1$). Moreover, the vehicle faces drag forces whose orientation is opposite

to the direction of the relative velocity $\mathbf{1}_{v-w} = (v-w)/\|v-w\|$. The direction of the lift force is given by $\mathbf{1}_k = k/\|k\|$ where the vector k reads

$$k = (\mathbf{1}_{v-w} \times \mathbf{1}_b) \times \mathbf{1}_{v-w}. \tag{4}$$

Meanwhile, the magnitudes of aerodynamic forces are modeled as functions of the angle-of-attack α and the Mach number $M = \|v-w\|/v_s(r)$, using the lift coefficient $C_L(\alpha, M)$ and the drag coefficient $C_D(\alpha, M)$, namely,

$$\begin{cases} L(r, v-w, \alpha) &= \frac{1}{2}\rho(r) S_{\text{ref}} C_L(\alpha, M) \|v-w\|^2, \\ D(r, v-w, \alpha) &= \frac{1}{2}\rho(r) S_{\text{ref}} C_D(\alpha, M) \|v-w\|^2. \end{cases} \tag{5}$$

In our model, $v_s(r)$ is the sound velocity in the air at the position r, and α designates the angle between the principal axis of the vehicle $\mathbf{1}_b$ and the relative velocity vector $v-w$. While studying VTVL problems,[9] it was shown that the computation of the optimal control can be facilitated by using a specific formulation of the aerodynamic coefficients.[20] An analogous operation is here performed by assuming that

$$\begin{cases} C_L(\alpha, M) &= C_{L_1}(M)\sin(2\alpha), \\ C_D(\alpha, M) &= C_{D_0}(M) + 2C_{L_1}(M)\sin^2(\alpha), \end{cases} \tag{6}$$

where $C_{L_1} = (C_{N_\alpha} - C_{D_0})/2$, with C_{N_α} the gradient of the lift coefficient in the body frame, and C_{D_0} is the drag coefficient for a null angle of attack. Given that $k = \mathbf{1}_b - \langle \mathbf{1}_b, \mathbf{1}_{v-w}\rangle \mathbf{1}_{v-w}$, the acceleration can be rewritten as

$$a = \Lambda \frac{T(r)}{m}\mathbf{1}_b + \frac{\rho(r)\|v-w\| S_{\text{ref}}}{2m}\Big(2C_{L_1}\langle \mathbf{1}_b, (v-w)\rangle \mathbf{1}_b - C_{N_\alpha}(v-w)\Big) - g(r). \tag{7}$$

Notice that the dynamic model of the considered RLV is broadly similar to the dynamics used for the recovery of VTVL vehicles.[9] Due to the relatively low lift-to-drag ratios of those configurations, it was possible to obtain a decent modeling with constant values for C_{N_α} and C_{L_1}. However, the vehicles addressed in our study may achieve a higher aerodynamic performance. In order to cover relevant configurations, we model the coefficients C_{N_α} and C_{L_1} as functions of the Mach number M.

2.2 Optimal control problem

Our goal is to recover a winged vehicle from a fixed initial state (r_0, v_0, m_0) to a given final configuration $\left(r_f^{\text{ref}}, v_f^{\text{ref}}\right)$ while minimizing propellant mass consumption along the return trajectory. In practice, the desired terminal configuration is chosen in order to guarantee a straightforward landing maneuver. While the vehicle is required to end its course at a specified position near the landing site, its final velocity must be correctly oriented towards the runway. Additionally, path constraints must be enforced on the angle-of-attack α, as well as the dynamic pressure

$$\bar{q} = \frac{1}{2}\rho(r)\|v\|^2, \tag{8}$$

the longitudinal load factor

$$n_x = \|\langle n, \mathbf{1}_b\rangle\|, \tag{9}$$

and the lateral load factor

$$n_z = \|n \times \mathbf{1}_b\|. \tag{10}$$

Here, n denotes the load factor of the engine which is given by $n = (a+g)/\|g\|$. Such a problem can be addressed with an optimal control problem,

$$\min \int_0^{t_f} \Lambda \,\mathrm{d}t + \frac{k_{r_f}}{2}\left\|r(t_f) - r_f^{\text{ref}}\right\|^2 + \frac{k_{v_f}}{2}\left\|v(t_f) - v_f^{\text{ref}}\right\|^2 \text{ s.t.} \left| \begin{array}{l} (r, v, m) \text{ follows the dynamics (1)}, \\ (r, v, m)(0) = (r_0, v_0, m_0), \\ t_f, r\left(t_f\right), v\left(t_f\right) \text{ and } m\left(t_f\right) \text{ are free}, \\ \alpha \in [0, \alpha_{\max}] \text{ if } \|r\| \le r_{\min}, \\ n_x \le n_{x,\max}, n_z \le n_{z,\max}, \bar{q} \le \bar{q}_{\max}. \end{array} \right. \tag{11}$$

Here, the vehicle is controlled by $(\Lambda(t), \mathbf{1}_b(t))$ whereas the cost function sums an integral term and a term dependent on the final state of the vehicle. While the integral term budgets the propellant consumption, our performance index

includes penalties on both the terminal position error and the terminal velocity error. Since the vehicle cannot make use of its rocket engine in order to adjust its velocity at the end of the trajectory, a fixed final velocity vector would be difficult to obtain, especially when the initial configuration of the vehicle at stage separation is uncertain. The objective function then includes a penalization on the final configuration $(\boldsymbol{r}(t_f), \boldsymbol{v}(t_f))$. Such an endpoint cost function allow us to trade between a feasible control problem (i.e. an admissible solution exists) and the reach of a desired velocity.[9,17] The vector $\boldsymbol{r}_f^{\text{ref}}$ (*resp.* $\boldsymbol{v}_f^{\text{ref}}$) then designates a reference value of the final position (*resp.* velocity) while k_{r_f} and k_{v_f} are tuning parameters. The reference configuration $\left(\boldsymbol{r}_f^{\text{ref}}, \boldsymbol{v}_f^{\text{ref}}\right)$ is typically selected so that a straightforward landing maneuver is possible.

Furthermore, the optimal control problem (11) involves pure state constraints (the dynamic pressure) and mixed control-state constraints (the load factors and the angle-of-attack). In practice, the angle-of-attack of the vehicle should not exceed a given value $\alpha_{\max}$ which typically depends on the Mach number M. In addition, such limitation makes sense when the engine hits dense regions of the atmosphere. A threshold altitude $r_{\min}$ is then defined and the constraint on the angle-of-attack is specified below this altitude. Given that the winged vehicle may perform multiple turns in order to align with the runway, the lateral load constraint will be a major concern.

2.3 Solution of the optimal control problem

We derive the optimal solution of the problem (11) through an application of the PMP[19,23] which reformulates the optimal control problem as a zero-finding problem.[8,19,23] First, the state of the vehicle $(\boldsymbol{r}, \boldsymbol{v}, m)$ is augmented by a co-state vector $(\boldsymbol{p_r}, \boldsymbol{p_v}, p_m)$ whose variations can be deduced from the Hamiltonian associated to the system:

$$H = \Lambda\left(1 - q_m p_m + \frac{T(\boldsymbol{r})}{m}\left\langle \boldsymbol{p_v}, \mathbf{1_b}\right\rangle\right) - \left\langle \boldsymbol{p_v}, \boldsymbol{g}(\boldsymbol{r})\right\rangle + \left\langle \boldsymbol{p_r}, \boldsymbol{v}\right\rangle + \frac{\rho(\boldsymbol{r})\left\|\boldsymbol{v}-\boldsymbol{w}\right\| S_{\text{ref}}}{2m}\Big[2C_{L_1}\left\langle \boldsymbol{v}-\boldsymbol{w}, \mathbf{1_b}\right\rangle\left\langle \boldsymbol{p_v}, \mathbf{1_b}\right\rangle - C_{N_\alpha}\left\langle \boldsymbol{p_v}, \boldsymbol{v}-\boldsymbol{w}\right\rangle\Big] - 2\left\langle \boldsymbol{p_v}, \boldsymbol{\Omega}\times\boldsymbol{v}\right\rangle - \left\langle \boldsymbol{p_v}, \boldsymbol{\Omega}\times(\boldsymbol{\Omega}\times\boldsymbol{r})\right\rangle. \quad (12)$$

The dynamics of the co-state vector are

$$\frac{\mathrm{d}}{\mathrm{d}t}\begin{pmatrix}\boldsymbol{p_r}\\ \boldsymbol{p_v}\\ p_m\end{pmatrix} = -\begin{pmatrix}\partial_{\boldsymbol{r}}\tilde{H}\\ \partial_{\boldsymbol{v}}\tilde{H}\\ \partial_m\tilde{H}\end{pmatrix}, \quad (13)$$

where $\tilde{H}$ is an extended Hamiltonian which includes the constraints, namely

$$\tilde{H} = H + \mu_\alpha\left(\alpha - \alpha_{\max}\right) + \mu_x\left(n_x - n_{x,\max}\right) + \mu_z\left(n_z - n_{z,\max}\right) + \mu_{\bar{q}}\left(\bar{q} - \bar{q}_{\max}\right). \quad (14)$$

Here μ_α, μ_x, μ_z and $\mu_{\bar{q}}$ denote Lagrangian multipliers.

Optimality necessary conditions The necessary conditions that are relevant for our study are listed below:

- The optimal control $(\Lambda(t), \mathbf{1_b}(t))$ minimizes the Hamiltonian H for all t.
- Since the final time t_f is free and knowing that the endpoint cost function does not depend on the time t,

$$H(t_f) = 0. \quad (15)$$

- The Hamiltonian H is constant since the dynamics (1) and the integral cost function do not explicitly depend on the time t.
- Given that $\boldsymbol{r}\left(t_f\right)$, $\boldsymbol{v}\left(t_f\right)$ and $m\left(t_f\right)$ are free, the following transversality conditions can be deduced.

$$\begin{pmatrix}\boldsymbol{p_r}\\ \boldsymbol{p_v}\\ p_m\end{pmatrix}\left(t_f\right) = -\begin{pmatrix}k_{r_f}\left(\boldsymbol{r}(t_f) - \boldsymbol{r}_f^{\text{ref}}\right)\\ k_{v_f}\left(\boldsymbol{v}(t_f) - \boldsymbol{v}_f^{\text{ref}}\right)\\ 0\end{pmatrix}. \quad (16)$$

- By assuming that the constraints are regular, the Lagrangian multipliers in Equation (14) are continuous mapping such that $\mu_\alpha\left(\alpha - \alpha_{\max}\right) = 0$, $\mu_x\left(n_x - n_{x,\max}\right) = 0$, $\mu_z\left(n_z - n_{z,\max}\right) = 0$ and $\mu_{\bar{q}}\left(\bar{q} - \bar{q}_{\max}\right) = 0$ for all t. Note that at every contact t_i with the boundary of the constraint on the dynamic pressure, a jump condition may apply on the co-state vector. Precisely, there exists $\nu_i \geq 0$ such that

$$\begin{cases} \boldsymbol{p_r}\left(t_i^+\right) - \boldsymbol{p_r}\left(t_i^-\right) &= -\nu_i \partial_{\boldsymbol{r}} \bar{q}, \\ \boldsymbol{p_v}\left(t_i^+\right) - \boldsymbol{p_v}\left(t_i^-\right) &= -\nu_i \partial_{\boldsymbol{v}} \bar{q}. \end{cases} \tag{17}$$

Multiple shooting method In practice, the necessary conditions listed above define a two-point boundary value problem which can be reformulated as a root-finding problem where the function for which the zero is sought depends on the initial value of the co-state vector $(\boldsymbol{p_r}, \boldsymbol{p_v}, p_m)$. A shooting algorithm thus integrates both the state dynamics (1) and the co-state dynamics (13) in order to evaluate the function whose zero is searched. Fast algorithms such as Newton-like methods[11] are then employed for the search of zeros. Although high numerical accuracy can be achieved with a modest computational effort, the classical limitation of the shooting method comes from its initialization. In order to mitigate this limitation, a multiple shooting method has been retained for the present study. This technique provides a robust solution by adding some intermediate knots and continuity conditions to the root-finding problem. Another advantage of the multiple shooting approach is its ability to deal with jump conditions induced by state constraints using contact points (see Eq. (17)) as well as switching times involved by bang arcs.[10,23]

Continuation method The initialization problem can be further addressed using continuation procedures.[6,9] We then solve a series of shooting problems which are indeed step by step deformations starting from a simplified version of the optimal control problem in order to reach the solution of the complete problem. At each step, the initialization is performed with the latest computed solution. The main challenge here resides in the choice of a sufficiently smooth deformation that allows the convergence of the method. The initial problem must be easy to solve, and the path between the simplified problem and the complete problem must be easy to model.[14] For our work, continuation procedures have been utilized for two purposes. First, an off-line reference trajectory is computed by a series of continuations starting from the same simplified optimal problem as for the VTVL recovery concept.[9] The off-line trajectory is a solution of the optimal control problem (11) where a wind free model is used and where initial conditions correspond to the vehicle configuration at the beginning of the recovery. Then, the onboard guidance performs continuations on both the initial conditions and the wind profile in order to match the current vehicle data (vehicle state, wind estimation).

Expression of the optimal control The optimal control theory dictates that the optimal control input $(\Lambda(t), \mathbf{1}_{\boldsymbol{b}}(t))$ is given by a minimization of the Hamiltonian H.[7,19,23] To achieve this minimization, one may take advantage of the expected structure of the optimal solution. The glide-back recovery can be depicted in two main phases.

- **Powered phase**: During this phase, the aerodynamic forces can be neglected since the vehicle is located at a relatively high altitude. Minimizing H can then be achieved with the minimization of the expression

$$J_1(\Lambda, u) := \Lambda\left(1 - q_m p_m + \frac{T(\boldsymbol{r})}{m}\left\langle \boldsymbol{p_v} \,.\, \mathbf{1}_{\boldsymbol{b}} \right\rangle\right). \tag{18}$$

  Therefore, the direction of the optimal thrust is given by

$$\mathbf{1}_{\boldsymbol{b}} = -\frac{\boldsymbol{p_v}}{\|\boldsymbol{p_v}\|}. \tag{19}$$

  Replacing $\mathbf{1}_{\boldsymbol{b}}$ by eq. (19) in eq. (18) gives

$$J_1 = \Lambda\psi. \tag{20}$$

  where ψ defines a switching function

$$\Psi = 1 - q_m p_m - \frac{T(\boldsymbol{r})}{m}\|\boldsymbol{p_v}\|. \tag{21}$$

  The thrust intensity thus has a Bang-Off profile. When $\Psi < 0$, the Hamiltonian H is minimal when the thrust force is maximized (i.e. $\Lambda = 1$). Conversely, the engines must be turned off (i.e. $\Lambda = 0$) as soon as $\Psi > 0$. The case where $\Psi = 0$ is irrelevant in this paper as we assume there is no singular trajectory. Thus, Ψ is never equal to zero on a non-empty interval. In practice, the function Ψ characterizes the switching time that separates the powered phase and the glide phase.

- **Unpowered or glide phase**: When the propulsion is switched off, aerodynamic forces can no longer be neglected. As a result, the minimization of the Hamiltonian H is given by minimizing

$$J_2(u) := \frac{\rho(\boldsymbol{r})\,\|\boldsymbol{v}-\boldsymbol{w}\|\,S_{\text{ref}}C_{L_1}(M)}{m}\,\langle \boldsymbol{v}-\boldsymbol{w}, \mathbf{1}_{\boldsymbol{b}}\rangle\,\langle \boldsymbol{p}_{\boldsymbol{v}}, \mathbf{1}_{\boldsymbol{b}}\rangle\,. \tag{22}$$

The optimal unit vector $\mathbf{1}_{\boldsymbol{b}}$ then lies in the plane $(\boldsymbol{p}_{\boldsymbol{v}}, \boldsymbol{v}-\boldsymbol{w})$ and

$$\mathbf{1}_{\boldsymbol{b}} = \frac{\|p_v\|\,(\boldsymbol{v}-\boldsymbol{w}) - \|\boldsymbol{v}-\boldsymbol{w}\|\,\boldsymbol{p}_{\boldsymbol{v}}}{\|\|p_v\|\,(\boldsymbol{v}-\boldsymbol{w}) - \|\boldsymbol{v}-\boldsymbol{w}\|\,\boldsymbol{p}_{\boldsymbol{v}}\|}. \tag{23}$$

Modification of the control input due to constraints Moreover, in order to handle path constraints, some modifications must be applied to the control input. Here, the pure state constraint on the dynamic pressure is treated with a contact point that splits the glide phase into two sub-phases. The expression of the control is identical in both sub-phases and follows Equation (23). However, a contact time $t_{\bar{q}}$ is introduced between these sub-phases. This time marks the contact with the stress $\left(\bar{q}(t_{\bar{q}}) = \bar{q}_{\max}\right)$ and thus follows the jump conditions provided by PMP (see Equation (17)).

Likewise, mixed constraints (angle-of-attack, load factors) are handled with saturations. Given the structure of the glide-back recovery, the saturations of the longitudinal load factor may occur in the powered phase while the constraints on both the lateral load factor and the angle-of-attack may be activated during the glide phase. Given that $\mathbf{1}_{\boldsymbol{b}}$ lies in the plane $(\boldsymbol{p}_{\boldsymbol{v}}, \boldsymbol{v}-\boldsymbol{w})$, the angle-of-attack constraint is straightforward to handle.[9] Furthermore, while neglecting the effect of the Earth's rotation, the lateral load factor can be linked to the value of the angle-of-attack. When the lateral load factor constraint becomes active ($n_z = n_{z,\max}$), a corresponding value of the angle-of-attack can be retrieved. This value is then utilized to determine the saturated control. In the same way, the longitudinal load factor can be linked to the engine throttle Λ during the powered phase. The activation of the constraint on the longitudinal load factor then induces a saturation of Λ.

Note that, when any mixed constraint becomes active, the dynamics of the co-state vector (see Equation (13)) require an explicit computation of the related Lagrangian multiplier. Given $\tilde{H} = 0$ for all t, the adequate value of the Lagrangian multipliers throughout the saturation can be deduced from $\mathrm{d}\tilde{H}/\,\mathrm{d}t = 0$ for all t.[9]

3. Navigation component with on-the-fly wind estimate

Throughout the recovery flight, the online guidance algorithm may require a representative estimation of the wind profile in order to compute a reliable optimal control. During the propelled phase, the winged vehicle can overcome any local uncertainty on the wind profile since the aerodynamic forces are negligible at that altitude. The focus should therefore be on the atmospheric phase. In order to derive a recursive state estimator such as Kalman filters, the wind $\boldsymbol{w}$ is added to the list of state variables. In Equation (7), the wind is no longer seen as a simple parameter. Meanwhile, we can assume that $\boldsymbol{w}$ is a state variable which follows a zero mean random process whose fluctuations are to be estimated. In the following, the state of the system during the atmospheric phase is denoted by $X(t) = (\boldsymbol{r}, \boldsymbol{v}, \boldsymbol{w})$ and $U(t) = \mathbf{1}_{\boldsymbol{b}}$ designates the control input. Here, we deliberately omit the dynamics of the mass since the latter remains constant during the atmospheric phase. Likewise, with the engines off, the vehicle body axis is genuinely the only control input. From the point of view of the navigation component, the physical system is then represented by a continuous-time model and the system state is monitored with discrete-time measurements (Z_k)

$$\begin{cases} \dot{X}(t) = f(X(t), U(t)) + \Sigma(t) \\ \\ Z_k = h\left(X\left(t_k\right)\right) + \Pi_k \end{cases}. \tag{24}$$

Here, the dynamics $f(X(t), U(t))$ derives from Equation (1), namely,

$$f(X(t), U(t)) = \begin{pmatrix} \boldsymbol{v} \\ \boldsymbol{a} - 2\boldsymbol{\Omega}\times\boldsymbol{v} - \boldsymbol{\Omega}\times(\boldsymbol{\Omega}\times\boldsymbol{r}) \\ \mathbf{0} \end{pmatrix}, \tag{25}$$

while both the process noise $\Sigma(t)$ and the observation noise Π_k are assumed to be zero mean multi-variate Gaussian noises with covariance $Q(t)$ and R_k respectively. In practice, on-board measurements provide information on the vehicle position and velocity. A classical application of Kalman filters is navigation where the vehicle position and velocity are

estimated using data from inertial measurement unit (IMU) and a global navigation satellite system (GNSS) receiver.[24] For our study, the following observation model has been used

$$h(X) = \begin{pmatrix} 1 & 0 & 0 \\ 0 & 1 & 0 \end{pmatrix} \begin{pmatrix} \boldsymbol{r} \\ \boldsymbol{v} \\ \boldsymbol{w} \end{pmatrix} = \begin{pmatrix} \boldsymbol{r} \\ \boldsymbol{v} \end{pmatrix}. \tag{26}$$

It is worth mentioning that for the considered problem, the use of both position and velocity observations is not mandatory. Indeed, observability conditions are fully satisfied as soon as we use the position data. Moreover, the presence of non-linearities in the dynamics (25) led us to the design of an extended Kalman filter. The method consists of applying the standard Kalman filter (for linear systems) to nonlinear systems with additive white noise by continuously updating a linearization around the previous state estimate, starting with an initial guess. The application of such an approach does not arise any major difficulty and the method has been thoroughly described in the literature.[5,13,21,24]

4. Numerical experiments

This section evaluates the efficiency of our algorithm by recovering the first-stage for a typical Sun-synchronous orbit (SSO) mission, launched from Kourou, French Guiana. We consider a winged vehicle whose aerodynamic lift-to-drag ratio may reach about 4 in subsonic regime. The recovery procedure begins while the vehicle is located about 60 km above the sea. The range of the vehicle is about 80 km away from the spaceport. The initial mass of the vehicle is 70 t and the recovery is subject to the following constraints: $\alpha_{\max} = 15\,\text{deg}$, $n_{x,\max} = 7.5$, $n_{z,\max} = 7$ and $\bar{q}_{\max} = 70\,\text{kPa}$. During its descent, the vehicle must be slowed down from about $2\,\text{km}\,\text{s}^{-1}$ to about $100\,\text{m}\,\text{s}^{-1}$, when the landing guidance algorithm would take over (∼1 km altitude). Specific algorithms are readily available for this particular landing phase (see *e.g.*[1,2,25]). Although the landing phase is not covered by our study, we orient the desired terminal velocity so that the vehicle can reach a given runway of the spaceport while maintaining its heading.

We computed off-line a reference trajectory that describes the motion of the vehicle throughout the recovery under nominal conditions with no wind disturbances. This trajectory is then used for the initialization of the online guidance algorithm.

We then performed two types of assessment. First, the vehicle is simulated in a more realistic environment with randomly scattered parameters (for example, initial state dispersion, aerodynamic coefficients, maximal thrust, maximal mass flow rate, air density, atmospheric pressure, etc.). These simulations were performed in the absence of wind in order to validate our implementation of the guidance component (see Section 4.2 for further details). Next, we specifically address the effect of wind in the recovery of winged vehicles by conducting simulations under wind profiles that are characteristic of typical flight conditions. For these simulations, the vehicle is positioned in a nominal initial state while the environmental parameters (pressure, density, etc.) remain scattered. The wind profiles were generated while including moderate gusts in accordance with aerospace guidelines.[15] Section 4.1 briefly describes the generation of those wind profiles. Under these conditions, the complete guidance algorithm has then been assessed with and without the wind estimate in the navigation component. Section 4.3 discusses the corresponding results.

4.1 Wind models

In order to validate our guidance method, which relies on an in-flight estimation of the wind profile, the vehicle must be exposed to sufficiently realistic wind models. For a conventional launcher, the effect of wind disturbance throughout the atmospheric phase is a critical factor that can lead to the loss of the vehicle.[18,22] This concern is even more prominent in the case of a winged recovery. We therefore rely on wind models that have proven their efficiency in the design of small launchers (i.e. VEGA) which are highly sensitive to winds. For this study, Dryden wind turbulence models[12,16] are used in order to generate wind components in both South-North and West-East directions. The wind disturbance velocity v_w is modeled with a colored white noise through a Dryden filter:

$$G_w(s,h) = \frac{v_w}{n_w}(s) = \frac{\sqrt{\frac{2(V(h)-w_0(h))}{\pi L(h)}\sigma^2(h)}}{s + \frac{V(h)-w_0(h)}{L(h)}}, \tag{27}$$

where n_w is a white noise. $L(h)$ and $\sigma(h)$ are the turbulence length scale and the standard deviation versus altitude h. w_0 is a build-up wind speed envelope described with an exponential leading edge for low altitudes, a constant value for

intermediates altitudes and a cosine shape trailing edge for high altitudes:

$$w_0(h) = \begin{cases} 10A\left[\left(\frac{h}{H_l}\right)^{0.9} - 0.9\frac{h}{H_l}\right] & \text{for} \quad 0 \le h \le H_l \\ A & \text{for} \quad H_l \le h \le H_f - H_u \\ \frac{A}{2}\left[1 - \cos\left(\frac{\pi(h-H_f)}{H_u}\right)\right] & \text{for} \quad H_f - H_u \le h \le H_f \end{cases} \tag{28}$$

These parameters can be tuned in order to generate various levels of turbulence (light, moderate, severe) following aerospace guidelines.[15] In order to mimic moderate wind gusts,[18] the envelope covers the first 20 km and we set the constant gust amplitude A to $14\,\mathrm{m\,s^{-1}}$. Meanwhile, the thickness of the initial edges are $H_l = 2\,\mathrm{km}$ and $H_u = 2.5\,\mathrm{km}$. The corresponding values of $L(h)$ and and $\sigma(h)$ are readily available in.[18]

4.2 Simulation results of the guidance algorithm with scattered parameters

Monte-Carlo simulations were conducted for 200 random configurations where the vehicle initial state as well as various environmental parameters were scattered. The simulations were performed in absence of wind and the guidance algorithm was successfully able to recover the vehicle up to its intended location.

Despite dispersions exceeding more than 50 km on the starting position, the algorithm was able to bring the vehicle within less than 50 m from the final reference position. The final speed is also satisfactory, since we only observe deviations of a couple of $\mathrm{m\,s^{-1}}$ from the targeted value (see Figure 3). In addition, in all cases, the winged vehicle is properly aligned with the runway. The final flight-path-angle and the final azimuth are within one degree of their desired values. While traveling to the runway, the vehicle complies with all path constraints (see Figure 4).

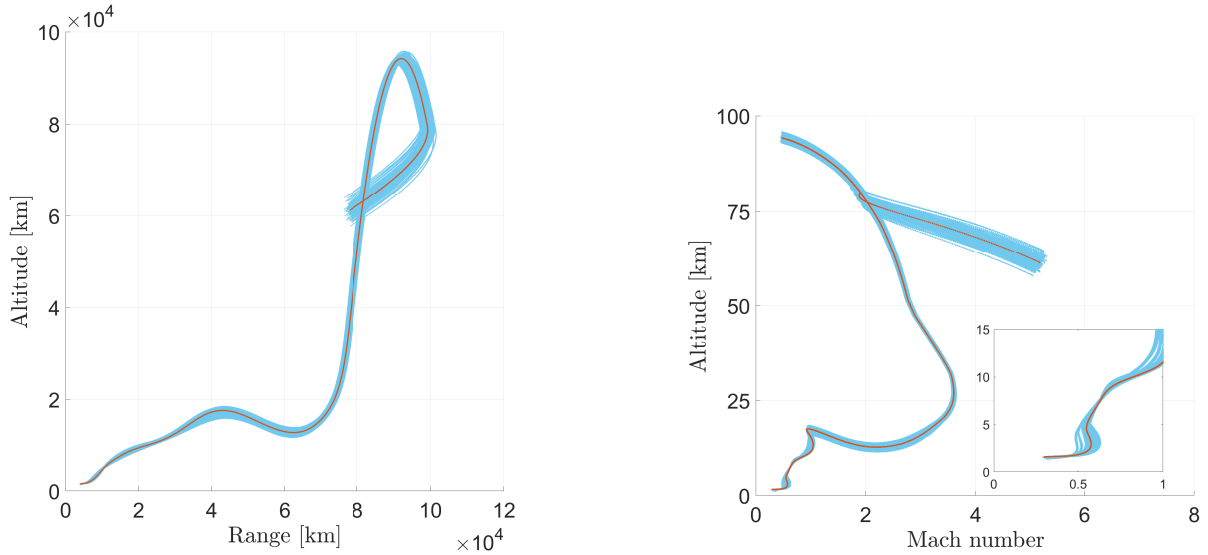

(a) Altitude vs Range

(b) Altitude vs velocity

Figure 3: Monte Carlo simulations with scattered parameters

4.3 Simulation results of the guidance algorithm in presence of wind

A glide-back recovery strategy exposes the vehicle to wind disturbances. We simulate such flight conditions by applying 200 wind profiles to the vehicle during the atmospheric phase of the return flight. In order to specifically isolate the atmospheric disturbances, the vehicle is placed in a nominal configuration (position, speed, engine) at the beginning of the recovery. For each simulation, a wind profile including moderate gusts is used along dispersions of atmospheric parameters (air density, pressure). The guidance algorithm is first used without any wind estimate. Then the scenario is replayed with wind estimate enabled in the navigation component. In the first case, the guidance algorithm is fully affected by the wind perturbations, while the use of the current wind estimate allows the guidance algorithm to compensate wind effects.

Figure 5 outputs the longitude vs latitude profiles of the obtained trajectories. The nominal trajectory without wind disturbance is presented in red while wind disturbed simulations are presented in blue. Figure 5a shows that

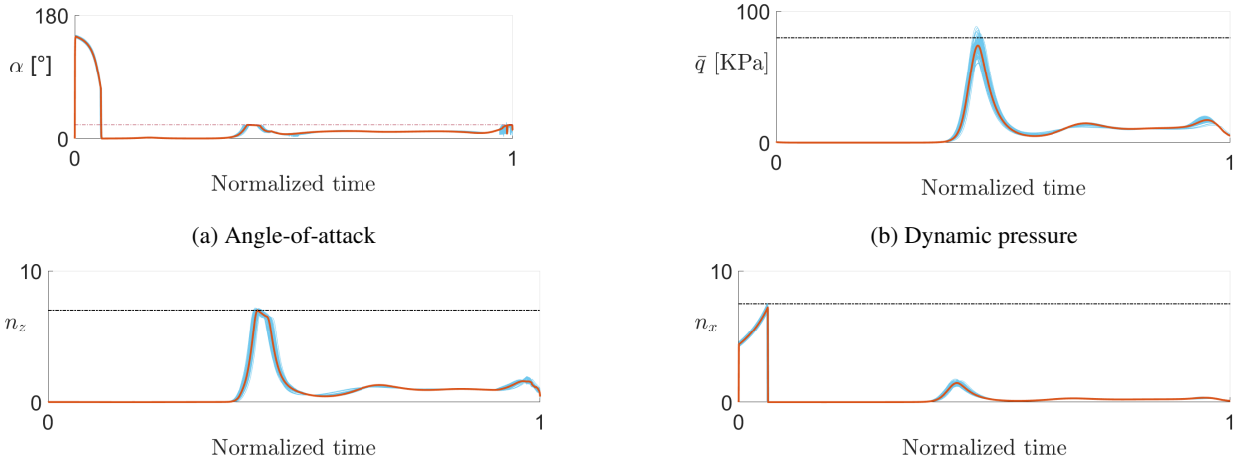

(a) Angle-of-attack

(b) Dynamic pressure

(c) Lateral load factor

(d) Longitudinal load factor

Figure 4: Path constraints from Monte Carlo simulations

wind disturbances produce substantial lateral drifts when the guidance algorithm does not take advantage of the on-the-fly wind estimate. These drifts affect the final turn made by the vehicle to align itself with the track. In most cases, however, the guidance algorithm is able to bring the vehicle to a reasonable distance from the aimed point. The standard deviation on the final position is about 200 m. Unfortunately, we note that in some cases the final state of the vehicle is not satisfactory. Some simulations have led to a final altitude far below the nominal target and a final velocity that may be either misdirected or too far off the desired value (Figure 6a).

The use of wind estimate results in a significant improvement of the guidance algorithm. From one end to the other, the obtained trajectories remain close to the nominal trajectory (Figure 5b). This, in turn, improves the completion of the final turn and allows the vehicle to terminate its journey within 40 m of the intended final position. Besides, the orientation of the final velocity vector is more consistent with a safe landing maneuver. The deviations of the final flight-path-angle and the final azimuth do not exceed 1 deg. At the same time,Figure 6b shows that the final speed remains consistent with its nominal value.

Moreover, the inclusion of wind estimate in the guidance scheme enables a better control of the path constraints throughout the flight. By analyzing the load factor profiles, we observe that the algorithm reduces the increase of the lateral load factor induced by crosswind gusts (Figure 7). A similar conclusion can be drawn from the analysis of the dynamic pressure profiles. A reduction in the dispersion of the dynamic pressure is noticed as soon as the wind estimate is used (Figure 8). The correction for headwind and tailwind effects is behind this observation.

In Figure 9, we output in East-North-Up frame the wind estimate obtained from a wind disturbed simulation. The disturbances are displayed with dots while solid lines output the on-the-fly wind estimate. The navigation block appears to perform well in estimating all components of the disturbance. While the wind estimates in the West-East direction are almost perfect, a slight delay is observed for the South-North component. We believe that the reason for this is related to the route followed by the vehicle during its recovery. Indeed during a major part of the flight (prior to the final turn), the vehicle flies in the North-South direction. The east wind disturbances thus appear as crosswind gusts. The response of the vehicle corresponds almost instantaneously to a lateral deviation which is easily detected by the Kalman filter. The north wind component is then perceived as headwind or tailwind gusts. The effects of such gusts are more difficult to read as they may be intermingled with fluctuations in atmospheric density profiles. These atmospheric disturbances are clearly apparent in the vertical component of the diffused wind, especially at the peak of dynamic pressure. The guidance algorithm then unwittingly compensates for certain disturbances in the density profile.

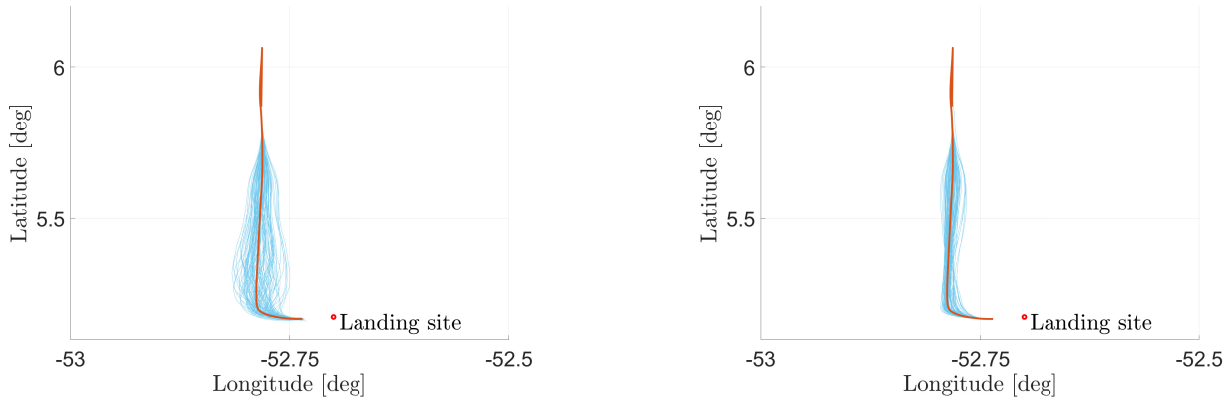

(a) Wind estimate disabled

(b) Wind estimate enabled

Figure 5: Wind disturbed simulations: Longitude-latitude profile

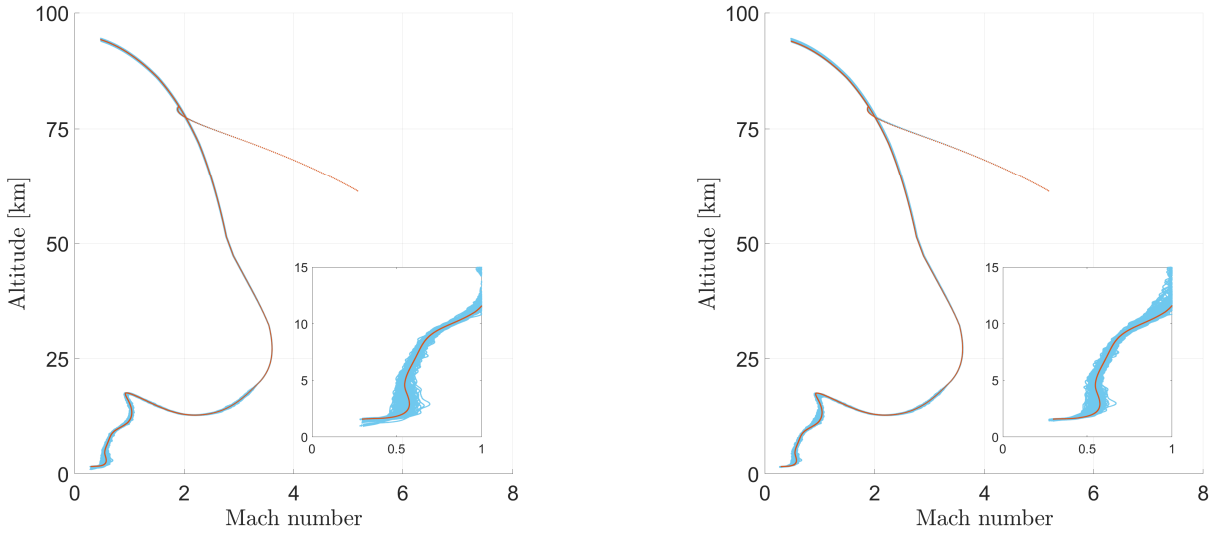

(a) Wind estimate disabled

(b) Wind estimate enabled

Figure 6: Wind disturbed simulations: Altitude vs Velocity profiles

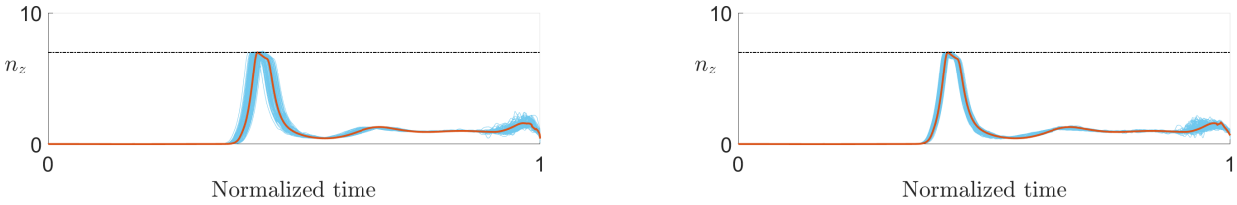

(a) Wind estimate disabled

(b) Wind estimate enabled

Figure 7: Wind disturbed simulations: Lateral load factor

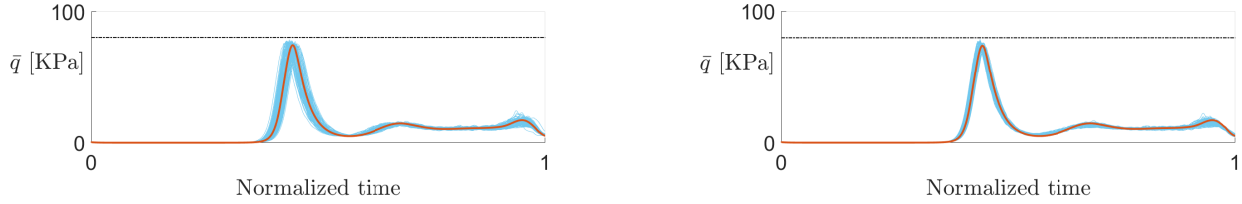

(a) Wind estimate disabled

(b) Wind estimate enabled

Figure 8: Wind disturbed simulations: Dynamic pressure

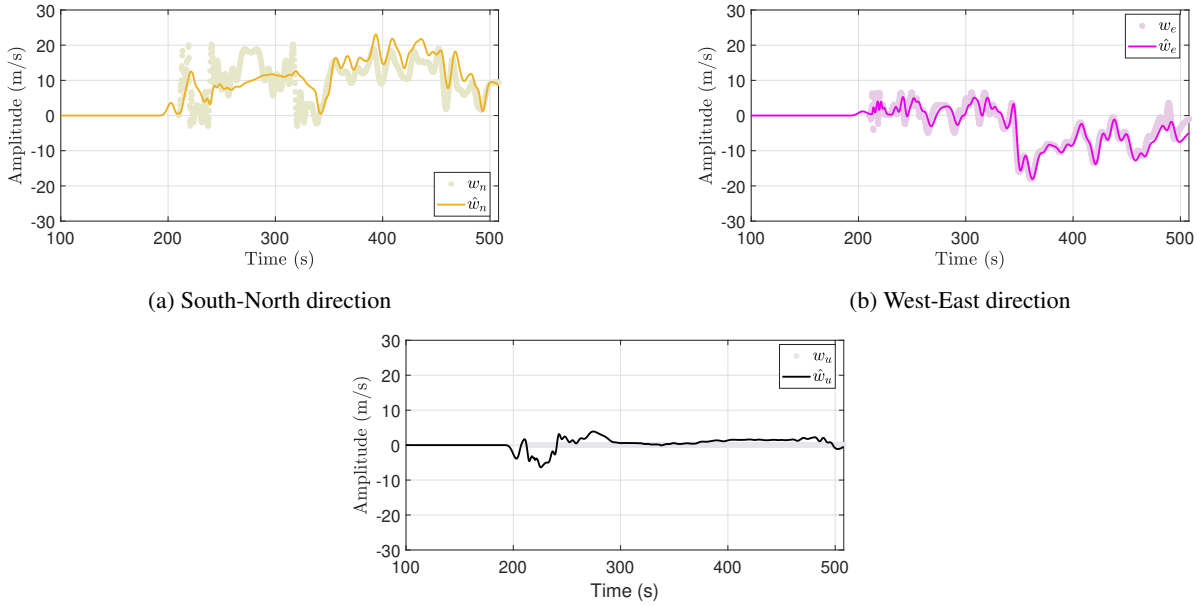

(a) South-North direction

(b) West-East direction

(c) Down-Up direction

Figure 9: Wind estimate from a wind disturbed simulation: *The disturbances are displayed with dots while solid lines output the on-the-fly wind estimate.*

4.4 Conclusion

This indirect shooting method based on Pontryagin's Maximum Principle has been successfully applied to the re-entry of a vertical take-off and horizontal landing vehicle. The main challenge was to provide a trajectory which allows a safe horizontal landing while minimizing the consumed mass and complying with path constraints. Given that winged return strategies are sensitive to atmospheric perturbations, the algorithm embeds a compensation of the wind disturbances when computing the optimal control. The algorithm can be paired with an on-the-fly wind estimate in order to build a closed-loop guidance algorithm which has been simulated in a more realistic physical environment. First, the model and mission parameters were scattered in order to demonstrate the efficiency of our implementation, which converged in 100% of the cases. Then, the vehicle was exposed to moderate wind gusts through several missions. The inclusion of an estimate of wind disturbances has significantly enhanced the robustness of the guidance algorithm. The wind estimate is efficiently provided by an extended Kalman filter. The wind estimate provided by the extended Kalman filter allows the vehicle to thwart the effects of gusty winds. As a consequence, excessive loads are mitigated throughout the flight.

Nevertheless, some aspects of our modeling are worth improving. First, the guidance model assumes that the instantaneous wind measurement provided by the navigation block remains constant throughout the descent. This strong assumption can lead the vehicle to maneuver in anticipation of a given wind direction on the lower atmospheric layers and that this initial steering backfires as we get closer to the ground. This side effect is well controlled with moderate gusts but might become threatening under strong gusty conditions. An improvement would be to include the the wind information acquired during the ascent phase. The guidance system could correct the actual wind against this

reference. Furthermore, a more realistic model of the system should be considered (i.e. rocket engine transient effects, etc.). Finally, it would be interesting to combine our algorithm with dedicated techniques for the landing phase.

References

[1] F. F. Al-Bakri, A. F. Al-Bakri, and C. A. Kluever. Approach and landing guidance for an unpowered gliding vehicle. *Journal of Guidance, Control, and Dynamics*, 43(12):2366–2371, 2020.

[2] F. F. AL-Bakri and C. A. Kluever. Automatic Approach and Landing Trajectory Planner for Unpowered Reusable Launch Vehicle. *Advances in Aerospace Science and Technology*, 02(04):31–47, 2017.

[3] P. Baiocco and C. Bonnal. Technology demonstration for reusable launchers. *Acta Astronautica*, 120:43–58, 2016.

[4] M. Balesdent, L. Brevault, B. Paluch, R. Wuilbercq, N. Subra, R. Thépot, and A. Patureau de Mirand. Design and optimization of glide-back reusable launch vehicle architectures. In *EUCASS 2019, Madrid, Spain*, July 2019.

[5] G. Bishop, G. Welch, et al. An introduction to the kalman filter. *Proc of SIGGRAPH, Course*, 8(27599-23175):41, 2001.

[6] R. Bonalli, B. Hérissé, and E. Trélat. Analytical initialization of a continuation-based indirect method for optimal control of endo-atmospheric launch vehicle systems. *IFAC-PapersOnLine*, 50(1):482–487, 2017.

[7] F. Bonnans, P. Martinon, and E. Trélat. Singular arcs in the generalized Goddard's problem. *Journal of Optimization Theory and Applications*, 139(2):439–461, 2008.

[8] B. Bonnard, L. Faubourg, G. Launay, and E. Trélat. Optimal control with state constraints and the space shuttle re-entry problem. *Journal of Dynamical and Control Systems*, 9(2):155–199, 2003.

[9] E. Brendel, B. Hérissé, and E. Bourgeois. Optimal guidance for toss back concepts of Reusable Launch Vehicles. In *EUCASS 2019*, July 2019.

[10] A. E. Bryson and Y.-C. Ho. *Applied optimal control: optimization, estimation, and control*. Routledge, 2018.

[11] A. Galántai. The theory of newton's method. *Journal of Computational and Applied Mathematics*, 124(1-2):25–44, 2000.

[12] T. M. I. Hakim and O. Arifianto. Implementation of dryden continuous turbulence model into simulink for lsa-02 flight test simulation. In *Journal of Physics: Conference Series*, volume 1005, page 012017. IOP Publishing, 2018.

[13] S. Haykin. *Kalman filtering and neural networks*, volume 47. John Wiley & Sons, 2004.

[14] A. Hermant. Optimal control of the atmospheric reentry of a space shuttle by an homotopy method. *Optimal Control Applications and Methods*, 32(6):627–646, 2011.

[15] D. L. Johnson. Terrestrial environment (climatic) criteria guidelines for use in aerospace vehicle development, 1993 revision. *NASA Technical Memorandum*, 4511, 1993.

[16] H. W. Liepmann. On the application of statistical concepts to the buffeting problem. *Journal of the Aeronautical Sciences*, 19(12):793–800, 1952.

[17] P. Lu. Propellant-optimal powered descent guidance. *Journal of Guidance, Control, and Dynamics*, 41(4):813–826, 2018.

[18] D. Navarro-Tapia, A. Marcos, P. Simplício, S. Bennani, and C. Roux. Legacy recovery and robust augmentation structured design for the VEGA launcher. *International Journal of Robust and Nonlinear Control*, 29(11):3363–3388, 2019.

[19] L. S. Pontryagin. *Mathematical Theory of Optimal Processes*. CRC Press, 2018.

[20] D. Pucci, T. Hamel, P. Morin, and C. Samson. Nonlinear feedback control of axisymmetric aerial vehicles. *Automatica*, 53:72–78, 2015.

[21] M. I. Ribeiro. Kalman and extended kalman filters: Concept, derivation and properties. *Institute for Systems and Robotics*, 43:46, 2004.

[22] P. Simplício, S. Bennani, A. Marcos, C. Roux, and X. Lefort. Structured singular-value analysis of the Vega launcher in atmospheric flight. *Journal of Guidance, Control, and Dynamics*, 39(6):1342–1355, 2016.

[23] E. Trélat. Optimal Control and Applications to Aerospace: Some Results and Challenges. *Journal of Optimization Theory and Applications*, 154(3):713–758, 2012.

[24] E. Wan. Sigma-point filters: An overview with applications to integrated navigation and vision assisted control. In *2006 IEEE Nonlinear Statistical Signal Processing Workshop*, pages 201–202. IEEE, 2006.

[25] X. Yan and L. He. Unpowered approach and landing trajectory planning using second-order cone programming. *Aerospace Science and Technology*, 101:105841, 2020.